5
Robustness of Oscillations: The Case of Solar Neutrinos

Early attempts to account for the solar neutrino problem proposed that the models of the Sun were incorrect: for example, that the temperature in the solar interior was substantially different from what was then believed. However, improved neutrino measurements as well as advances in helioseismology, namely the study of how waves propagate through the Sun, have by now made such possibilities untenable. For example, such helioseismology observations allow us to measure the interior temperatures of the Sun, which is in good agreement with the standard solar models (SSMs). On the other hand, detailed observations of the solar neutrino spectrum obtained at Super-K and other neutrino observatories also produced results that cannot be reconciled with changes in the solar model.

Historically, there were several mixing parameter sets that could account for the solar neutrino results: the large mixing angle (LMA), small mixing angle (SMA), low mass (LOW) and vacuum oscillations (VAC). However, with time, various measurements were carried out that became good enough to rule out all of these solutions except for the LMA region (see the summary plot of the 'landscape' of solar neutrino oscillation parameters given in Figure 4.17).

In fact, one may argue that the very good precision achieved in the experiments is such that solar neutrino data may be used to learn about the Sun's properties, in other words, to obtain information of direct astrophysical relevance. For example, the measurement of neutrino properties at KamLAND provides valuable information about fluctuations in the solar environment on scales to which standard helioseismic constraints are largely insensitive.

All in all, neutrino physics has undergone a profound revolution over the last 15 years or so. Experiments observing neutrinos produced inside the Sun, in the Earth's atmosphere, in nuclear power plants and in particle accelerators have finally established the existence of a new phenomenon called *neutrino oscillations*, a quantum effect expected when neutrinos have mass. In the standard model of elementary particles, neutrinos are massless. Hence, the discovery of neutrino oscillations has far-reaching implications, since it is a clear evidence for physics beyond the standard $SU(3)_c \otimes SU(2)_L \otimes U(1)_Y$ model and requires an extension of the basic theory. These provide strong reasons to scrutinize how solid the oscillation discovery is from every possible viewpoint. For example, regarding solar neutrino conversions, we note that the oscillation description relies both on

Neutrinos in High Energy and Astroparticle Physics, First Edition. José W. F. Valle and Jorge C. Romão.

the physics characterizing the neutrino propagation and interaction properties, as well as on the astrophysical input provided by the solar model. These may differ from the standard electroweak model as well as the SSM expectations. In what follows, we focus upon some of these uncertainties. Taking for granted the current determinations of neutrino oscillation parameters, one may also infer the astrophysical implications about neutrino-emitting sources such as the Sun or supernovae.

One may explore also the robustness of the oscillation interpretation for the atmospheric neutrino data sample. Non-standard physics may, in principle, affect atmospheric neutrino fluxes as well as neutrino propagation and detection cross sections [73]. Here we focus only on the case of solar neutrinos.

5.1 Theoretical Preliminaries: Beyond the Standard Model

Generically, most models generating the neutrino masses that are required to make sense of the oscillation data described in the previous chapter also induce non-standard neutrino interactions, illustrated in Figure 5.1. The search for effects associated with these operators is important, as it would shed light upon the underlying mass scale and mechanism involved in neutrino mass generation. From the theory point of view, the physics responsible for neutrino masses could lie at the teraelectrovolt (TeV) scale. In this case, it is unlikely that neutrino masses are not accompanied at a certain level by some non-standard neutrino interactions. These could induce novel features in neutrino propagation as well as lepton-flavor-violating (LFV) processes involving the charged leptons.

The simplest form of NSI (non-standard interaction) arises from the $SU(3)_c \otimes SU(2)_L \otimes U(1)_Y$ electroweak gauge sector of seesaw-type schemes (Chapters 7, 13 and 14) as a result of lepton mixing effects in the weak neutral currents [46]. Generically, such NSIs may be parameterized with the effective low-energy four-fermion operator [73]

$$\mathcal{L}_{NSI} = -\epsilon^{fP}_{\alpha\beta} 2\sqrt{2} G_F (\overline{\nu}_\alpha \gamma_\mu L \nu_\beta)(\overline{f}\gamma^\mu P f), \tag{5.1}$$

where $P = L, R$ and f is a first-generation fermion: e, u, d. The coefficients $\epsilon^{fP}_{\alpha\beta}$ denote the strength of the NSI between the neutrinos of flavours α and β and the P-handed component of the fermion f.

The strength of such NSI operators is related to the scale and underlying mechanism responsible for giving mass to neutrinos. Other potentially sizeable NSI types may arise from the symmetry-breaking scalar sector associated with neutrino mass generation in gauge theories, such as in radiative models [105, 106], or supersymmetric extensions of the standard model [86]. These NSIs may, in principle, affect neutrino propagation properties within matter, leading to non-oscillatory neutrino flavour conversion [55–57] as well as lepton flavour and/or CP violation involving charged leptons, which may take place even in the massless neutrino limit [52–54].

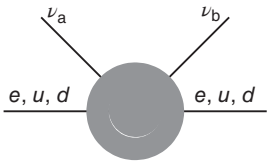

Figure 5.1 Generic non-standard interaction (NSI) operator, whose strength is related to the scale of the 'messengers' associated to neutrino mass generation.

Within the two-neutrino approximation, the Hamiltonian describing neutrino evolution in the Sun in the presence of matter and NSI contains, in addition to the standard oscillations term

$$\mathcal{H}_{\rm OSC} = \begin{bmatrix} -\frac{\Delta m^2}{4E}\cos 2\theta + \sqrt{2}\, G_F N_e & \frac{\Delta m^2}{4E}\sin 2\theta \\ \frac{\Delta m^2}{4E}\sin 2\theta & \frac{\Delta m^2}{4E}\cos 2\theta \end{bmatrix}, \tag{5.2}$$

a term $H_{\rm NSI}$ that includes the effective potential induced by the NSI with matter, which may be written as

$$\mathcal{H}_{\rm NSI} = \sqrt{2} G_F N_d \begin{bmatrix} 0 & \varepsilon \\ \varepsilon & \varepsilon', \end{bmatrix}, \tag{5.3}$$

where the effective parameters ε and ε' are related to the vectorial couplings as[1)]

$$\varepsilon = -\sin\theta_{23}\, \varepsilon^{dV}_{e\tau}, \qquad \varepsilon' = \sin^2\theta_{23}\, \varepsilon^{dV}_{\tau\tau} - \varepsilon^{dV}_{ee}, \tag{5.4}$$

where N_d in Eq. (5.3) is the number density of the down-type quark along the neutrino path. Note that the neutrino evolution inside the Sun and the Earth is sensitive only to the vector component of the NSI, $\varepsilon^{dV}_{\alpha\beta} = \varepsilon^{dL}_{\alpha\beta} + \varepsilon^{dR}_{\alpha\beta}$. The effect of the axial coupling is discussed in detail in Ref. [74].

Figure 5.2 shows the resulting neutrino survival probabilities averaged over the ^{8}B neutrino production region for the best fit points with and without NSI (see Ref. [251] for details). Lines are compared with the experimental rates for the pp neutrino flux, the 0.862-MeV ^{7}Be neutrino line (from Borexino) and two estimated values of the ^{8}B neutrino flux from Borexino and the Sudbury Neutrino Observatory (SNO) (third phase). The vertical error bars correspond to the experimental errors, while the horizontal ones indicate the energy range observed in each experiment.

As already discussed in Section 3.3.3, within the various seesaw-type schemes to be discussed in Chapters 7, 13 and 14, the lepton mixing matrix $\boldsymbol{V}^{\rm LEP} \equiv K$ is generally rectangular because the heavy neutrino 'messenger' states responsible for neutrino mass generation also couple to the charged leptons [46].

Even in low-scale seesaw realizations, where messengers can be relatively light, they still are expected to be too heavy to participate in neutrino oscillations. As a result, these would be described by an effective non-unitary 3×3 mixing matrix.[2)] Apart from novel features expected in neutrino propagation, the

1) This approximate two-neutrino description neglects θ_{13} and takes advantage of the stringent limits on $\varepsilon^{fP}_{\alpha\mu}$. For simplicity, we also assume absence of NSI with electrons and up-type quarks.
2) This constitutes perhaps the most basic theoretical origin for non-standard neutrino interactions.

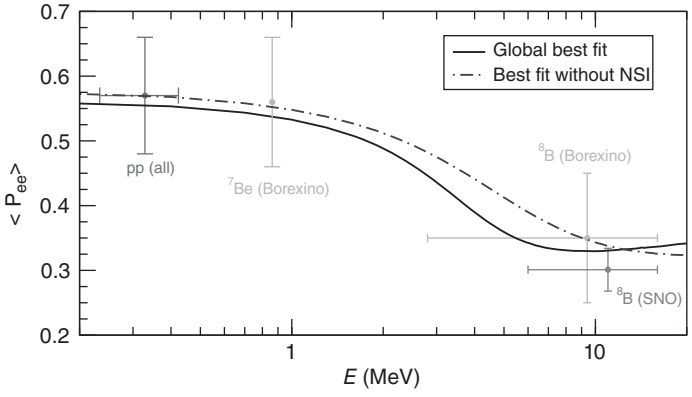

Figure 5.2 Neutrino survival probabilities with and without NSI, from Ref. [251].

non-trivial form of the charged current weak interaction in seesaw schemes would also induce LFV processes involving the charged leptons, avoiding the Glashow–Iliopoulos–Maiani (GIM) suppression [129].

While the charged lepton flavour violation has been extensively searched for, as will be seen in Chapter 15, searches for flavour violation in neutrino propagation beyond oscillations, are still in their infancy. However, these are in the agenda of current and upcoming experiments [252].

There is some level of correlation between both classes of phenomena, since neutrinos and charged leptons sit in doublets under the $SU(2)_L$ gauge group. However, gauge symmetry is broken so that, despite the expected correlation, one finds that non-unitarity in the lepton mixing matrix up to the percent level is still consistent with the current constraints that follow from charged lepton flavour violation searches in the laboratory. This fact is illustrated in Table 5.1, where we have parameterized the deviation from unitarity of the effective mixing matrix K_L by the small parameter η as in Ref. [253]

$$K_L \equiv (1-\eta)V, \tag{5.5}$$

where V is a unitary matrix.

In Table 5.1, we give limits on unitarity violation parameters from the current bounds on lepton flavour violation searches in the laboratory. This result holds within low-scale realizations of the type I seesaw mechanism, such as the inverse seesaw (labeled I) and the linear seesaw (labeled L) schemes to be discussed later in Sections 7.3.4 and 13.3. These limits express the correlation between lepton non-unitarity and lepton flavour violation observables, and hold even within the simplest 'minimal flavour violation' hypothesis (see Ref. [254] for details).

Note that the bounds in Table 5.1 are not especially stringent, so that upcoming long-baseline neutrino oscillation experiments [80] should also open the way towards complementary tests of lepton flavour violation in neutrino propagation.

Table 5.1 Limits from lepton flavour violation searches on unitarity violation parameters in normal hierarchy within simple low-scale seesaw schemes, labeled (I) and (L). Percent level deviations are allowed in most cases by current charged lepton flavour violation limits, from Ref. [254].

Process	$\mu \to e\gamma$	$\tau \to e\gamma$	$\tau \to \mu\gamma$
$\lvert\eta^I_{12}\rvert$	1.4×10^{-3}	2.8×10^{-2}	2.8×10^{-2}
$\lvert\eta^I_{13}\rvert$	2.0×10^{-2}	1.1×10^{-2}	3.1×10^{-2}
$\lvert\eta^I_{23}\rvert$	2.1×10^{-2}	6.4×10^{-2}	1.2×10^{-2}
$\lvert\eta^L_{12}\rvert$	9.6×10^{-4}	5.1×10^{-2}	5.3×10^{-2}
$\lvert\eta^L_{13}\rvert$	2.7×10^{-2}	1.1×10^{-2}	4.8×10^{-2}
$\lvert\eta^L_{23}\rvert$	2.2×10^{-2}	5.5×10^{-2}	1.2×10^{-2}

Indeed, it is likely that such future experiments will probe these unitarity deviation parameters, and hence the associated physics, which is complementary to that probed through weak universality tests and/or searches for rare lepton flavour violation processes. Note that non-standard neutrino interactions may also modify neutrino detection cross sections. As a result, their existence can affect the solar neutrino signal observed at various experiments. Also, from this point of view, it is important to scrutinize the robustness of the oscillation interpretation of current neutrino data *vis-a-vis* the possible existence of non-standard neutrino interactions. Upcoming long-baseline neutrino oscillation experiments, for example, at neutrino factories, should include in their agenda the task of probing for physics beyond oscillations, namely the interplay of oscillations with NSI effects [80, 255–257]. In order to take up this goal into account, future neutrino oscillation experiments will require the inclusion of near detectors as well as the optimization of their design configurations.

5.2
Beyond the Standard Solar Model

Here we address some of the astrophysical uncertainties associated with the possible presence of magnetic fields in the Sun, both in its radiative and convective zones. First, we note that the good agreement between the SSM sound speed profile and that deduced from helioseismology has made it harder to motivate substantial changes in the model [208, 258]. Yet, the effect of varying solar neutrino fluxes has been widely discussed and included in some of the analyses of neutrino oscillation parameters (see, e.g. the February 2010 arXiv version of Ref. [240]).

However, although experiments are now measuring neutrino fluxes to within a small percentage of precision, helioseismic maps of interior sound speeds have already reached accuracies of about a few parts in a thousand. Hence, it is not inconceivable that clashes may eventually appear [208, 258].

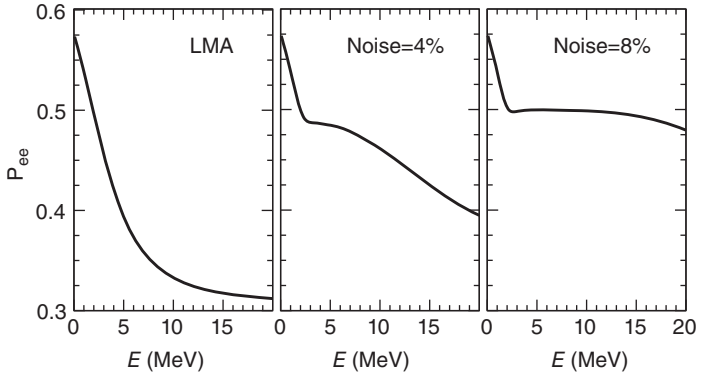

Figure 5.3 Effect of random matter density fluctuations with a correlation length of $L_0 =$ 100 km on the electron-neutrino survival probability for LMA oscillations. (Adapted from Ref. [259].)

We now discuss very briefly the implications of possible departures from the SSM associated with the possibility of solar density fluctuations, first suggested in a number of papers in the late 1990s [260, 261]. Preliminary studies of the implications for neutrino oscillations of radiative-zone helioseismic waves [262] indicated that they were unlikely to have sizeable effects in neutrino propagation. Moreover, no other known sources of fluctuations seemed to have the properties required to influence neutrino oscillations.

Subsequent studies indicated, however, that the presence of solar fluctuations seemed a more interesting possibility than previously thought. First, direct helioseismic bounds are insensitive to fluctuations whose size is around several hundreds of kilometres to which neutrinos are sensitive [263, 264]. Second, recent studies have shown how such solar density fluctuations can arise near the solar equatorial plane in the presence of magnetic fields deep within the solar radiative zone due to a resonance between Alfvén waves and helioseismic g-modes [265]. This could provide a physical mechanism for generating these fluctuations.

The effect of random matter density fluctuations on the electron–neutrino survival probability for LMA oscillations has been shown to be sizable if the correlation length L_0 is comparable to the neutrino oscillation length in the Sun [259]. Such density fluctuations can indeed affect neutrino propagation in an important way. This is illustrated in Figure 5.3. The fluctuation's amplitude ξ at the position of neutrino resonance is zero in the left panel, and is $\xi = 4\%$ and $\xi = 8\%$ in the middle and right panels, respectively. The corresponding solar neutrino oscillation parameters obtained in the global neutrino oscillation fit are shown in Figure 5.4. If only the solar data is included, one finds that the 'noise' effect is substantial, as seen by comparing the large contours in the figure with the noiseless determination considered in the previous chapter. However, once the KamLAND data are combined, only the small region in Figure 5.4 is allowed and there is hardly any

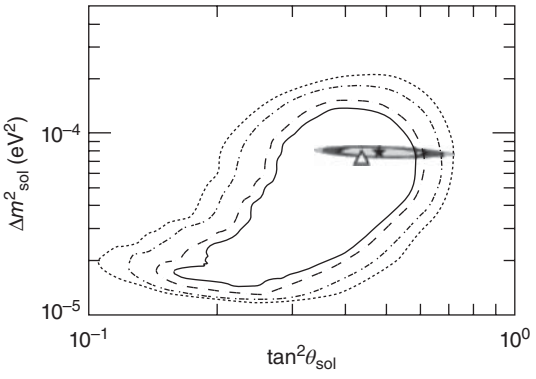

Figure 5.4 Solar neutrino oscillation parameters with an arbitrary 'noise' amplitude and a correlation length $L_0 = 100$ km. Although noise affects the solar region (large contours), there is hardly any effect left after combining with the KamLAND data (shaded contours). (Adapted from Ref. [266].)

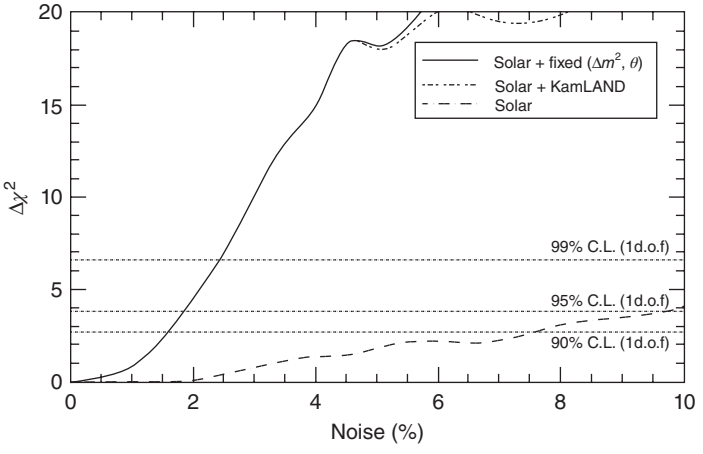

Figure 5.5 Bounds on random matter density fluctuations for a correlation length of $L_0 = 100$ km from solar neutrino data, solar + KamLAND data, and solar data for oscillation parameters fixed at the best fit point. (Adapted from Ref. [82].)

effect of the density noise whatsoever. This illustrates the importance of the KamLAND experiment in establishing the robustness of the solar neutrino parameter determination in this context.

Conversely, neutrino oscillation measurements can be used to constrain the size of magnetic fields deep within the solar radiative zone. Indeed, as shown in Ref. [266], the quality of current solar neutrino measurements and KamLAND results is good enough so as to place important constraints on the allowed level of fluctuations in the solar medium deep within the solar radiative zone. In other words, neutrino oscillation data may be used as an astrophysical probe of the solar interior, beyond the framework of the SSM.

As illustrated in Figure 5.5, density fluctuations are strongly constrained if the correlation length lies in the range of several hundreds of kilometres. Comparing the curves for free and fixed oscillation parameters, one notes that the bounds on fluctuations have already become as strong as they can get. Because oscillations are sensitive to correlation lengths which are so short, such solar neutrino results provide constraints complementary to those that come from helioseismology studies.

5.3 Oscillations with Spin-Flavour Precession

As already mentioned, in extensions of the standard model neutrino masses are in general accompanied also by novel neutrino interactions, a generic example of which is the dimension-6 operators we have briefly discussed in Section 5.1. Another example is provided by the neutrino's electromagnetic properties such as magnetic moments. In a gauge theory, these dimension-5 operators arise from Feynman diagrams such as the ones in Figure 5.6. In the minimal extension of the standard model with Dirac neutrino masses, one expects these to be very tiny because of the GIM suppression factor [267], well below conceivable experimental sensitivities. However, the general case of Majorana neutrinos [169] leads to potentially larger transition magnetic moments. This happens, for example, in some seesaw schemes with extra gauge and/or scalar interactions which may yield values closer to the present sensitivities. Leaving aside the model-dependent issue of the attainable magnitude of the transition moments, we note that they may

- affect neutrino propagation in the Sun beyond the oscillation mechanism because of the possible presence of solar magnetic fields in the convective zone;
- affect the determination of neutrino oscillation parameters because of non-standard neutrino cross sections inside the detectors.

Apart from modifying the propagation properties of neutrinos within the Sun, an interesting feature of the spin-flavour precession (SFP) mechanism is that, combined with oscillations (OSC), it necessarily implies the existence of an $\overline{\nu}_e$ component as part of the neutrino flux from the Sun reaching the detector. This is

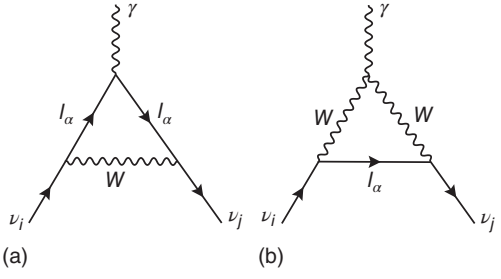

Figure 5.6 (a,b) Gauge contributions to the neutrino transition magnetic moments.

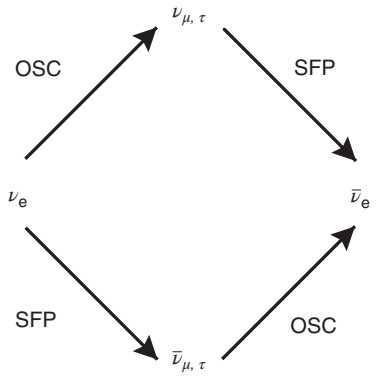

Figure 5.7 Solar anti-neutrinos produced through the interplay of spin-flavour precession (SFP) and oscillations (OSC) of solar neutrinos [169, 268, 269].

schematically illustrated in Figure 5.7. This flux can be searched experimentally, for example, at KamLAND. One finds, in some cases, a rather stringent constraint on the neutrino transition magnetic moments, as we will see below.

The general form of the electromagnetic current of massive (Majorana) neutrinos has been discussed in Chapter 3, Section 3.5.2. The magnetic piece is characterized by a 3×3 complex anti-symmetric matrix, the so-called Majorana transition moment matrix [169], that contains magnetic as well as electric dipole moments of the neutrinos [170, 188]. Their existence would affect neutrino propagation inside the solar convective zone as a result of an SFP effect.

As the simplest approximation, one may employ a two-neutrino picture of neutrino evolution, neglecting the angle θ_{13}. Solar neutrino evolution in the presence of a magnetic field involves then only the solar mixing angle where $\theta_{12} \equiv \theta_{sol} \equiv \theta$ and is described by a four-dimensional Hamiltonian [169, 268, 269]

$$i\begin{bmatrix} \dot{\nu}_{eL} \\ \dot{\bar{\nu}}_{eR} \\ \dot{\nu}_{aL} \\ \dot{\bar{\nu}}_{aR} \end{bmatrix} = \begin{bmatrix} V_e - c_2\delta & 0 & s_2\delta & \mu_\nu b_+(t) \\ 0 & -V_e - c_2\delta & -\mu_\nu b_-(t) & s_2\delta \\ s_2\delta & -\mu_\nu b_+(t) & V_a + c_2\delta & 0 \\ \mu_\nu b_-(t) & s_2\delta & 0 & -V_a + c_2\delta \end{bmatrix} \begin{bmatrix} \nu_{eL} \\ \bar{\nu}_{eR} \\ \nu_{aL} \\ \bar{\nu}_{aR} \end{bmatrix}, \tag{5.6}$$

where $\nu_a = \nu_\mu \cos\theta_{23} - \nu_\tau \sin\theta_{23}$, with $\theta_{23} \equiv \theta_{atm}$ the atmospheric mixing angle; $c_2 = \cos 2\theta$ and $s_2 = \sin 2\theta$; and $\delta = \Delta m^2/4E$ is assumed to be always positive. Here,

$$V_e(t) = G_F\sqrt{2}[N_e(t) - N_n(t)/2]$$

and

$$V_a(t) = G_F\sqrt{2}[-N_n(t)/2]$$

are the neutrino matter potentials for ν_{eL} and ν_{aL} in the Sun, specified by the electron and neutron number densities $N_e(t)$ and $N_n(t)$. Finally, $b_\pm = b_x \pm ib_y$ denote the magnetic field components which are perpendicular to the neutrino trajectory. Note that, in this approximation, the Majorana neutrino transition magnetic

moment element $\mu_\nu \equiv \mu_{ea}$ describing transitions between neutrino flavour states ν_e and ν_a coincides with the element μ_{12} characterizing transitions between mass eigenstates ν_1 and ν_2. Note that, inside the radiative zone, where the magnetic field is neglected, the evolution of the neutrinos reduces to that implied by large mixing oscillations. In order to get an approximate analytic solution for Eq. (5.6) in the convective zone, it is convenient to work in the mass basis.

Results will, in general, depend on the assumed magnetic field profile. Little is known about the detailed features of solar magnetic fields, and several models have been proposed [270, 271]. Different models make different assumptions about the nature of solar magnetic fields, which can be regular or random, and also about their magnitude, location and typical scales [272–276].

In order to determine the allowed regions of oscillation parameters in the presence of sub-leading SFP, one can perform a χ^2 analysis, as in Ref. [186], taking into account the global solar + KamLAND disappearance data samples. It is reasonable to assume that solar neutrino conversions are driven mainly by LMA oscillations. However, the magnetic fields in the solar convective zone will play a role. These can be modelled within a self-consistent approach [273] using the field profile employed in Ref. [218]. The results obtained indicate that, current bounds on the neutrino's magnetic moments and solar magnetic fields still leave room for slight modifications in the determinations of solar neutrino oscillation parameters, in the presence of large magnetic moments. Note that, while the analysis of solar neutrino data applies also to the special case of Dirac neutrinos, in the general Majorana case, where theory may give rise to higher moments, there is an additional characteristic feature of the SFP mechanism which will lead to more stringent constraints, namely the production of anti-neutrinos as illustrated in Figure 5.7. Here, one notes that the KamLAND collaboration [277] greatly improves the bound on an anti-neutrino component in the solar flux from 0.1% of the solar boron ν_e flux to 2.8×10^{-2}% at the 90% C.L., which is about 30 times better than the previous Super-K sensitivity [278]. The limits on solar electron anti-neutrino fluxes from Super-K and KamLAND are indicated by the horizontal lines in Figure 5.8. The limit on the intrinsic neutrino magnetic moment given by the tilted band has an intrinsic uncertainty associated with the turbulent magnetic field model and indicated by the width of the band. The crossing of this line with the lowest KamLAND line gives the limit $\mu_\nu = 5 \times 10^{-12} \mu_B$. For comparison, the vertical line indicates the present MUNU reactor limit. A more conservative and pessimistic limit discussed in Refs [186, 187] would give the limit indicated by the hatched band.

These results can be used to establish the robustness of the solar neutrino oscillation parameter determination. Assuming that random magnetic fields are of turbulent origin [271], one finds that the latter is rather stable against the possible existence of sub-leading SFP conversions. This implies that solar neutrino oscillation parameters may be inferred without much reference to intrinsic neutrino magnetic properties or solar magnetic fields. In contrast, for the case of Dirac neutrinos where this limit does not apply, the determination of oscillation parameters is potentially less robust. However, in this case we note that the gauge theoretic

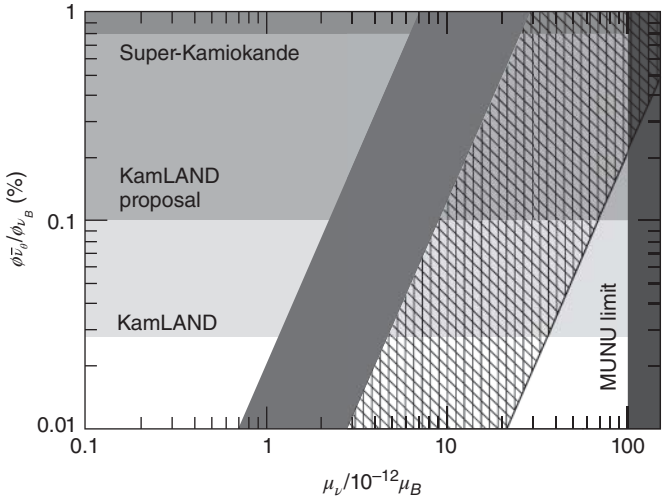

Figure 5.8 Bounds on μ_ν for the turbulent magnetic field model described in Refs [186, 187]. The horizontal lines indicate the bounds on solar electron anti-neutrino fluxes from Super-K and KamLAND, while the tilted band gives the limit on the intrinsic neutrino magnetic moment, its width corresponding to our turbulent magnetic field model uncertainties. The crossing of this line with the lowest KamLAND line gives the limit $\mu_\nu = 5 \times 10^{-12}\mu_B$. For comparison, the vertical line indicates the reactor limit from the MUNU experiment. A more conservative limit is indicated by the hatched band. (Taken from Ref. [187].)

expectations for strength of Dirac magnetic moments are much lower than those for Majorana neutrino transition moments.

All in all, one finds pretty good stability of the oscillation parameter determination for the case of Majorana neutrinos, due mainly to the solar anti-neutrino limit from KamLAND.

5.4
Constraining Neutrino Magnetic Moments

It is important to obtain information on intrinsic neutrino transition magnetic moments, as these constitute basic properties calculable within a given electroweak massive neutrino theory [169]. Although they do not substantially affect neutrino propagation, non-trivial electromagnetic neutrino properties could still show up in the detection process and to this extent affect the determination of oscillation parameters. Experiments based on the neutrino detection via neutrino–electron elastic scattering constitute a sensitive probe of the electromagnetic properties. In Ref. [279], it was shown how current solar neutrino data (e.g. from Super-K) in combination with reactor neutrino–electron scattering data constrain all the elements of the Majorana transition moment matrix (for similar analyses, see Ref. [280–283]). In several experiments such as Super-K,

Borexino and some reactor experiments [284–286], neutrinos are detected via the elastic neutrino–electron scattering, whose electromagnetic cross section is given as [287, 288]

$$\frac{d\sigma_{\rm em}}{dT} = \frac{\alpha^2\pi}{m_e^2\mu_B^2}\left(\frac{1}{T} - \frac{1}{E_\nu}\right)\mu_{\rm eff}^2, \tag{5.7}$$

where $\mu_{\rm eff}$ is an effective magnetic moment [289], T denotes the kinetic energy of the recoil electron and E_ν is the incoming neutrino energy. The electromagnetic cross section adds to the weak cross section and allows the extraction of information on the Majorana transition moment matrix, which we denote by λ in the following. Taking into account the antisymmetry of λ for Majorana neutrinos, it is useful to define vectors $\mathbf{\Lambda}$ by $\lambda_{jk} = \varepsilon_{jkl}\Lambda_l$, where λ_{jk} are the elements of the Majorana transition moment matrix in the mass basis, and

$$|\mathbf{\Lambda}|^2 = |\Lambda_1|^2 + |\Lambda_2|^2 + |\Lambda_3|^2.$$

The effective magnetic moment square $\mu_{\rm eff}^2$ takes on different forms for the cases of solar and reactor neutrino experiments; the relevant expressions are derived in Ref. [279]. For the case of solar neutrino experiments, one obtains the effective magnetic moment squared as

$$\mu_{\rm LMA}^2 = |\mathbf{\Lambda}|^2 - |\Lambda_2|^2 + P_{e1}^{2\nu}(|\Lambda_2|^2 - |\Lambda_1|^2), \tag{5.8}$$

where $P_{e1}^{2\nu}$ corresponds to the probability that an electron neutrino produced in the core of the Sun arrives at the detector as the mass eigenstate ν_1 in a two-neutrino scheme. In contrast, the $\mu_{\rm eff}^2$ relevant in reactor experiments is given as

$$\mu_{\rm R}^2 = |\mathbf{\Lambda}|^2 - \cos^2\theta_{\rm SOL}|\Lambda_1|^2 - \sin^2\theta_{\rm SOL}|\Lambda_2|^2 - \sin 2\theta_{\rm SOL}|\Lambda_1||\Lambda_2|\cos\delta, \tag{5.9}$$

where $\delta = \arg\,(\Lambda_1^*\Lambda_2)$ is the relative phase between Λ_1 and Λ_2. We now discuss the constraints on Majorana neutrino transition moments that come from solar and reactor neutrino experiments [279]. One constructs a χ^2 function from the relevant data and minimizes with respect to all Majorana transition moment parameters, except for the modulus $|\mathbf{\Lambda}|$. Such bounds apply to *all* elements of the Majorana transition moment matrix, including magnetic moments and electric dipole moments of all neutrino flavours, since $|\mathbf{\Lambda}|^2 = |\Lambda_1|^2 + |\Lambda_2|^2 + |\Lambda_3|^2$. Since $|\mathbf{\Lambda}|$ is basis-independent, these bounds also apply for the Majorana transition moment in the flavour basis.

In Figure 5.9, we show contours of the 90% C.L. bound on $|\mathbf{\Lambda}|$ in the $(\tan^2\theta_{\rm SOL}, \Delta m^2_{\rm SOL})$ plane for the combination of solar and reactor data. We note that, in the upper parts of the LMA region, the solar data alone give already a strong bound on $|\mathbf{\Lambda}|$ (see Ref. [279] for details). In contrast, for low $\Delta m^2_{\rm SOL}$ values, the inclusion of reactor data plays an important role in improving the bound. One finds the 90% C.L. limit

$$|\mathbf{\Lambda}| < \begin{cases} 3.4\times10^{-10}\mu_B & \text{(solar + KamLAND data)} \\ 1.7\times10^{-10}\mu_B & \text{(solar + KamLAND + reactor data),} \end{cases} \tag{5.10}$$

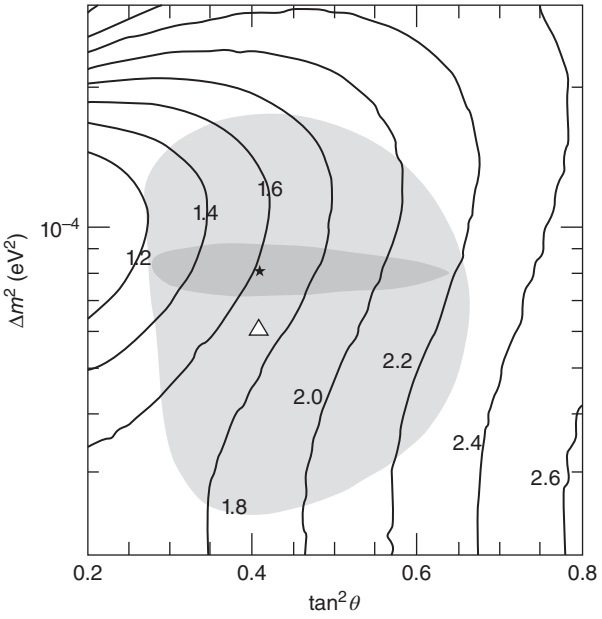

Figure 5.9 Contours of the 90% C.L. bound on $|\mathbf{\Lambda}|$ in units of $10^{-10}\mu_B$ from combined solar and reactor data. The light shaded region is the 3σ LMA region obtained in the global analysis of solar neutrino data (best fit point marked with a triangle), whereas the dark one corresponds to the 3σ region obtained after including the KamLAND results (best fit point marked with a star), from Ref. [82].

where for each value of $|\mathbf{\Lambda}|$ the χ^2 is minimized with respect to the solar oscillation parameters $\tan^2\theta_{\rm SOL}$ and $\Delta m^2_{\rm SOL}$.

Finally, we note that the sensitivity of the Borexino experiment [290] is roughly one order of magnitude better. This experiment is mainly sensitive to the solar ^{7}Be neutrino flux, measured by elastic neutrino–electron scattering. Therefore, Borexino is similar to Super-K, the main difference being the mono-energetic line of the ^{7}Be neutrinos, with an energy of 0.862 MeV, which is roughly one order of magnitude smaller than the energies of the ^{8}B neutrino flux relevant in Super-K. Thanks to the lower neutrino energy, the sensitivity to electromagnetic properties is enhanced, as can be seen from Eq. (5.7). Details about our Borexino simulation can be found in Ref. [279]. After 3 years of Borexino data collection, the expected sensitivity at the best fit point is

$$|\mathbf{\Lambda}| \leq 0.29 \times 10^{-10}\mu_B \quad \text{at} \quad 90\%\ \text{CL}. \tag{5.11}$$

For actual results from the Borexino collaboration, see Ref. [291].

5.5 Summary

In this chapter, we have seen that the neutrino oscillation interpretation of current neutrino data is fairly robust with regard to reasonable alternative assumptions made. We have explicitly considered the case of solar neutrinos, though the same also happens for atmospheric neutrinos. We now have a very good measurement of the three mixing parameters of the lepton mixing matrix which, to some extent, also constrains the presence of NSIs.

However, oscillation searches can only probe the two neutrino squared mass splittings, being insensitive to the absolute scale of neutrino masses. In the next chapter we address this issue.

5.6 Problems for Chapter 5

5.1 Parameterizing the NSI effective Hamiltonian by the coefficients $\epsilon_{e\alpha}$

$$\mathcal{H}_{\rm NSI} = \frac{G_F}{\sqrt{2}}[\overline{\nu}_\mu\ (1-\gamma_5)\gamma_\lambda\ \mu]\sum_\alpha \epsilon_{e\alpha}[\overline{e}\ (1-\gamma_5)\gamma^\lambda\ \nu_\alpha] + \text{h.}c., \tag{5.12}$$

show that the standard Fermi constant G_F, experimentally determined from the muon decay width is given as

$$G_F^{\rm exp} = G_F\left(|1+\epsilon_{ee}|^2 + \sum_{\alpha=\mu,\tau}|\epsilon_{e\alpha}|^2\right)^{1/2}. \tag{5.13}$$

Hint: note that the flavour of the neutrinos is not detected. The term ϵ_{ee} leads to exactly the same final state as the standard model process and must be added coherently, while $\epsilon_{e\mu}$ and $\epsilon_{e\tau}$ lead to different final states and contribute incoherently to the decay. One sees that the high-precision measurement of $G_F^{\rm exp}$ on its own does not directly constrain any of the parameters in Eq. (5.12); only the combination in Eq. (5.13) is constrained within the accuracy of the experimental measurement [21].

5.2 Show that, for the case of oscillations in the presence of neutrino non-standard interactions (OSC+NSI), Eq. (4.10) is modified to

$$\cos 2\theta_m = \frac{\Delta m^2\cos 2\theta - 2\sqrt{2}\,EG_F(N_e-\varepsilon' N_d)}{[\Delta m^2]_{\rm matter}}, \tag{5.14}$$

where

$$[\Delta m^2]^2_{\rm matter} = [\Delta m^2\cos 2\theta - 2\sqrt{2}\,EG_F(N_e-\varepsilon' N_d)]^2 + [\Delta m^2\sin 2\theta + 4\sqrt{2}\,\varepsilon\,EG_F N_d]^2. \tag{5.15}$$

Thanks to the presence of the non-universal coupling ε', one can obtain $P<0.5$ even for $\cos 2\theta<0$ as long as $\varepsilon' > \frac{2\sqrt{2}\,EG_F N_e+\Delta m^2|\cos 2\theta|}{2\sqrt{2}\,EG_F N_d}$. This makes it possible to

explain the solar neutrino data for values of the vacuum mixing angle in the dark side, for large enough values of ε'. As shown in Ref. [74], this possibility leads to the appearance of another LMA solution with $\theta > \frac{\pi}{4}$ and thus may allow for an ambiguous determination of the solar mixing angle. Analyse which measurements have the potential to rule out this possibility.

5.3 Consider the charged-current Lagrangian

$$\mathcal{L}_{\rm CC} = -\frac{g}{\sqrt{2}} W_\mu \bar{e}_{aL} \gamma^\mu K_{ai} \nu_{iL} + \text{h.c.}, \; a = e, \mu, \tau, \qquad i = 1, 2, 3, \quad (5.16)$$

where the effective mixing matrix $K \equiv R\mathcal{N}$ is the product of a diagonal matrix $\mathcal{N} = \text{diag}(\mathcal{N}_1, \mathcal{N}_2, \mathcal{N}_3)$ times a 3×3 rotation matrix R, and hence non-unitary [55]. The corresponding form of the neutral-current Lagrangian is

$$\mathcal{L}_{\rm NC} = -\frac{g}{2\cos\theta_W} Z_\mu P_{ij} \bar{\nu}_{iL} \gamma^\mu \nu_{jL} \,, \quad (5.17)$$

where $P = K^\dagger K \equiv \mathcal{N}^2 \equiv (1 + h_i^2)^{-1}, i = 1, 2, 3$. Unlike in the standard model, the matrix P is diagonal but non-degenerate, signalling the violation of weak universality. The parameters h_i reflect the deviation from the standard neutrino couplings and are constrained by experiments probing weak universality not to exceed a small percentage for the case of ν_τ and more stringent for ν_μ [21]. Take for simplicity the case of two neutrinos. The above weak currents describe a system of two massless non-orthogonal neutrinos, since

$$\langle \nu_e | \nu_{\mu,\tau} \rangle \equiv -\sin\theta \cos\theta (\mathcal{N}_1^2 - \mathcal{N}_{2,3}^2). \quad (5.18)$$

Write the system of Schrödinger equations describing the evolution of the two-neutrino system and show the existence of a massless-neutrino resonant conversion, provided the following resonance condition holds:

$$Y_e = \eta Y_n, \quad (5.19)$$

where the small parameter $\eta \equiv \frac{1}{2}(h_e^2 - h_\tau^2)$ characterizes $e - \tau$ universality violation. Observe that

- the resonance condition is not fulfilled in the Sun but may hold in a strongly neutronized medium such as certain regions of a supernova in its late cooling phase;
- if the resonance takes place, it converts neutrinos and anti-neutrinos simultaneously, in contrast to the standard MSW mechanism;
- the resulting neutrino survival probability is independent of the neutrino energy.

Hint: note that the resonance happens when the diagonal entries of the evolution Hamiltonian equal each other.